Cogn Comput (2013) 5:281–294
DOI 10.1007/s12559-013-9214-3

Neural 'Bubble' Dynamics Revisited

Paul C. Bressloff · Stephen Coombes

Received: 20 August 2012 / Accepted: 14 March 2013 / Published online: 28 March 2013
© The Author(s) 2013. This article is published with open access at Springerlink.com

Abstract In this paper, we revisit the work of John G Taylor on neural 'bubble' dynamics in two-dimensional neural field models. This builds on original work of Amari in a one-dimensional setting and makes use of the fact that mathematical treatments are much simpler when the firing rate function is chosen to be a Heaviside. In this case, the dynamics of an excited or active region, defining a 'bubble', reduce to the dynamics of the boundary. The focus of John's work was on the properties of radially symmetric 'bubbles', including existence and radial stability, with applications to the theory of topographic map formation in self-organising neural networks. As well as reviewing John's work in this area, we also include some recent results that treat more general classes of perturbations.

Keywords Neural field models · Self-organisation · Bumps · Breathers

Reflections

PCB I first met John in 1985 when he interviewed me for a PhD. position in string theory at King's College London. I had drifted away from academia at the time and was thus grateful that he decided to offer me the position. I was immediately struck by his sharpness, his larger-than-life personality, and his enthusiasm for mathematics and science. Although that enthusiasm would sometimes lead John to follow rather controversial paths, it was inspiring for a young graduate student. When I started my PhD, John had a large group of students working on horrendous perturbation calculations in supergravity. I still remember the long line of students disappearing down the corridor waiting to discuss their latest results. However, all of these students graduated during my first year so I was essentially John's only student, which meant that we worked closely together. My thesis work formed part of a book on 'Finite Superstrings' [49] co-authored with John and one of his long-standing collaborators Alvarez Restuccia from Venezuela. After graduating, I joined the Long-range Research Lab at the Hirst Research Center in London, which carried out fundamental research for GEC-Marconi. I was asked to develop a research programme in neural networks, which coincidentally was a research area that John had embraced in the 1970s and returned to in the late 1980s. John became a research consultant for GEC-Marconi and this enabled us to continue collaborating. Unfortunately, John and I lost contact when I joined Loughborough University in 1993. In fact, I only saw John one more time, which was as a guest speaker at his 'retirement' colloquium. Of course, John remained as active as ever following his retirement, in particular, pursuing his lifetime fascination with the problem of consciousness.

SC I was a PhD student with John from 1991–1994 at King's College London together with a large cohort of other students, including Dan Allen, Neil Taylor, Rasmus Petersen, Paulo Adeodato, Bart Krekelberg, Oury Monchi, and Simon Hastings. My work at that time was concerned with investigating the computational ability of higher-order

P. C. Bressloff
Department of Mathematics, University of Utah, Salt Lake City, Utah 84112, USA
e-mail: bressloff@math.utah.edu

S. Coombes (✉)
Department of Mathematical Sciences, Center for Mathematical Medicine and Biology, University of Nottingham, Nottingham NG7 2RD, UK
e-mail: stephen.coombes@nottingham.ac.uk

neurons (artificial single neuron models that could compute polynomial functions of their input) and recurrent networks of Hopfield type. This latter work involved statistical mechanical calculations of storage capacity, as well as the development of learning rules. John strongly encouraged me to think about the relevance of this work to hippocampal processing, which set me on the path to investigate the dynamics of biological, as opposed to artificial, neural networks. Since then, I have never looked back! I have very fond memories of my time at King's, including the realisation within a few days of starting my PhD on neurocomputing that John was none other than the author of 'Black Holes: The End of the Universe?' [47], a popular science book that I had enjoyed reading as a teenager. I became aware that I was joining his group at a time when his research activity was moving primarily from topics in mathematical physics to the mathematical theory of neural networks. Although I never worked with John on neural field models and 'bubble' dynamics, it is a pleasure to describe, with Paul, some of his work on this topic as well as more recent progress in this area. It is a rare treat to have met someone as vibrant as John and with such broad-ranging scientific interests. I will miss his mellifluous tones.

Introduction

In this paper, we revisit a problem that John considered in 1999 [48], namely the existence and stability of radially symmetric spots in two-dimensional (2D) neural fields, also known as 'neural bubble dynamics'. Neural fields represent the large-scale dynamics of spatially structured networks of neurons in terms of nonlinear integrodifferential equations, whose associated integral kernels represent the spatial distribution of neuronal synaptic connections. One type of solution that emerges in the presence of nonlocal synaptic inhibition (lateral inhibition) is a stationary spot solution, also known as an activity bump. Such bumps are typically coexistent with a stable low-activity state (bistability) so that an initial stimulus is needed in order to transition from the low-activity state to the bump. However, the bump persists after removal of the stimulus, so that the bump represents a persistent spatially localised activity state [12, 24, 33]. One of the reasons why persistent activity bumps are of interest is that they are thought to arise in cortical circuits performing certain spatial working memory tasks. Working memory involves cortical "memory neurons" that establish a representation of a stimulus that persists after the stimulus is removed. A typical experiment is a delayed response task, in which a primate is required to retain information regarding the location of a sensory cue across a delay period between the stimulus and behavioural response. Physiological recordings in prefrontal cortex have shown that spatially localised groups of neurons fire during the recall task and then stop firing once the task has finished [22]. The stimulus response of a cell is characterised by a smooth tuning curve that is peaked at a preferred spatial cue and varies from cell to cell. At the network level, the memory of cue location is stored as an activity bump. Persistent activity bumps occur in a number of other systems that encode directional or spatial information, including head direction cells in thalamus and basal ganglia [46] and place cells in the hippocampus [38].

Prior to John's study [48], almost all analyses of bumps had been restricted to 1D networks. Wilson and Cowan established the existence of 1D bumps numerically [53, 54], and Amari subsequently constructed an exact bump solution for a 1D scalar neural field equation with a Heaviside firing rate function [1]. He also showed how the stability of the bump depends on whether or not perturbations of the bump boundary (threshold crossing points) grow or decay. Interestingly, Amari also developed an analysis of 2D bumps. However, this work only appeared in a 1978 book that was never translated from the Japanese [3] and has only just been summarised in English [5]. John generalised Amari's 1D analysis by deriving conditions for the existence of radially symmetric 2D bumps and by determining the stability of the bumps with respect to radially symmetric perturbations of the circular bump boundary [48], see also [50]. This analysis was later extended to the case of nonradially symmetric perturbations using Fourier methods and properties of Bessel functions [16, 20, 21, 25, 39]. In related work, Laing and Troy [32] introduced PDE methods to study symmetry breaking of rotationally symmetric bumps and the formation of multiple bump solutions. However, such PDE methods can only be applied to specific forms of weight distribution. In particular, they break down if the weight distribution has compact support.

In section 'Dynamics of a 'Bubble' Boundary', we review the work of John (in an appropriately revised notation) on 2D bumps, as well as describe how to treat azimuthal instabilities, and the generation of breathing bumps in neural field models with adaptation and external drive. Next in section 'Self-Organising Neural Field Theory' we cover John's work on how 2D bump activity can drive topographic map formation in self-organising neural networks, also presented in [48], and describe a further set of techniques for treating nonradially symmetric perturbations. We end with a brief discussion in section 'Discussion'.

Dynamics of a 'Bubble' Boundary

Consider the following neural field equation for a 2D sheet of neural tissue

$$\tau \frac{\partial u(\mathbf{r},t)}{\partial t} = -u(\mathbf{r},t) + \int_{\mathbb{R}^2} w(|\mathbf{r}-\mathbf{r}'|) f(u(\mathbf{r}',t)) \mathrm{d}\mathbf{r}' \tag{1}$$

where $\mathbf{r} = (r, \theta)$ and $\mathbf{r}' = (r', \theta')$. The neural field $u(\mathbf{r}, t)$ represents the local activity of a population of neurons at position $\mathbf{r}$, τ is a synaptic or membrane time constant (which we set to unity), w is the distribution of synaptic weights, and f denotes an output firing rate function. The weight distribution is assumed to depend on the Euclidean distance $|\mathbf{r} - \mathbf{r}'|$ between interacting neurons at $\mathbf{r}$ and $\mathbf{r}'$. A common choice for the firing rate function is a bounded, monotonic function such as a sigmoid. Here we follow Amari [1] and Taylor [48] and take this to be Heaviside function with threshold κ such that $f(u) = H(u - \kappa)$. Below we review John's extension of Amari's 1D analysis to radially symmetric localised solutions in 2D. For a more detailed discussion of methods for analysing the existence and stability of bumps in neural fields, see recent reviews by the authors [9, 14].

First let us rewrite the original model (1) in the form $u_t = -u + \psi$, where

$$\psi(\mathbf{r},t) = \int_{\mathcal{B}(\mathbf{r}',t)} \mathrm{d}\mathbf{r}' w(|\mathbf{r}-\mathbf{r}'|), \tag{2}$$

and $\mathcal{B}(\mathbf{r},t) = \{\mathbf{r}|u(\mathbf{r},t) \geq \kappa\}$ (which defines the 'bubble'). For radially symmetric spot solutions of radius $\Delta(t)$ then we have that $\psi(\mathbf{r}, t) = \psi(r, t)$ with

$$\psi(r,t) = \int_0^{2\pi} \mathrm{d}\theta \int_0^{\Delta(t)} w\left(\sqrt{r^2 + r'^2 - 2rr'\cos\theta}\right) r' \mathrm{d}r'. \tag{3}$$

Here $\Delta(t)$ is defined by the level set condition $u(\Delta(t), t) = \kappa$. Time-independent spot solutions such that $\Delta(t) = \Delta$ (namely with a constant radius) such that $u(\mathbf{r}, t) = U(r)$ with $\lim_{r\to\infty} U(r) = 0$ and $U(r) \gtrless \kappa$ for $r \lessgtr \Delta$ are given by

$$U(r) = \psi(r,t)|_{\Delta(t)=\Delta}. \tag{4}$$

Differentiating the level set condition with respect to time gives an equation for the velocity of the spot boundary in the form

$$\frac{\mathrm{d}\Delta}{\mathrm{d}t} = -\left.\frac{\partial u(r,t)/\partial t}{\partial u(r,t)/\partial r}\right|_{r=\Delta}. \tag{5}$$

Using (1) we may derive an ODE for $v = \partial u(r,t)/\partial r|_{r=\Delta}$ as

$$\frac{\mathrm{d}v}{\mathrm{d}t} = -v + \left.\frac{\partial \psi}{\partial r}\right|_{r=\Delta}. \tag{6}$$

Hence, we may generate a system of two exact nonlinear ODEs for (Δ, v) to describe the evolution of the (radially symmetric) spot:

$$\frac{\mathrm{d}\Delta}{\mathrm{d}t} = -\frac{-\kappa + \Psi(\Delta)}{v}, \quad \frac{\mathrm{d}v}{\mathrm{d}t} = -v + \Psi'(\Delta), \tag{7}$$

where

$$\Psi(\Delta) = \int_0^{2\pi} \mathrm{d}\theta \int_0^{\Delta} w\left(\sqrt{\Delta^2 + r^2 - 2\Delta r\cos\theta}\right) r\mathrm{d}r. \tag{8}$$

The steady state of (7) is determined by the solution of $\Psi(\Delta) = \kappa$ and $v = \Psi'(\Delta)$. A linear stability analysis around the steady-state solution shows that there are two eigenvalues, one with value -1 (that can not lead to any instability) and the other with a value λ, where

$$\lambda = -\Psi'(\Delta)/v. \tag{9}$$

Hence, only the solution with $\Psi'(\Delta) < 0$ is stable (after realising that v is the gradient of the spot at its boundary and is negative).

In the 'Appendix', we show that $U(r)$ can be written in the computationally useful form

$$U(r) = 2\pi\Delta \int_0^{\infty} \widehat{w}(\rho) J_0(\rho r) J_1(\rho\Delta) \mathrm{d}\rho, \tag{10}$$

where $\widehat{w}$ is the 2D Fourier transform of w. For the sake of illustration, consider a wizard hat weight distribution given by a combination of modified Bessel functions of the second kind

$$w(r) = \frac{2}{3\pi}(K_0(r) - K_0(2r) - A(K_0(r/\sigma) - K_0(2r/\sigma))). \tag{11}$$

As shown in Fig. 1, this can generate a weight distribution with short-range excitation and long-range inhibition. Using the fact that the corresponding 2D Fourier transform of $K_0(s\ r)$ is $\mathcal{H}(\rho, s) = (\rho^2 + s^2)^{-1}$, we have

$$\widehat{w}(\rho) = \frac{2}{3\pi}(\mathcal{H}(\rho,1) - \mathcal{H}(\rho,2) - A(\mathcal{H}(\rho,1/\sigma) - \mathcal{H}(\rho,2/\sigma))). \tag{12}$$

Thus, the integral (10) can be evaluated explicitly using the identity

$$\int_0^{\infty} \frac{J_0(\rho r) J_1(\rho\Delta)}{\rho^2 + s^2} \mathrm{d}\rho \equiv \mathcal{I}(\Delta, r, s) = \begin{cases} \frac{1}{s} I_1(s\Delta) K_0(sr) & r > \Delta \\ \frac{1}{s^2\Delta} - \frac{1}{s} I_0(sr) K_1(s\Delta) & r < \Delta, \end{cases} \tag{13}$$

where I_v is the modified Bessel function of the first kind of order v. Thus, the stationary bump $U(r)$ has the form

$$U(r) = \frac{4\Delta}{3}[\mathcal{I}(\Delta,r,1) - \mathcal{I}(\Delta,r,2) - A(\mathcal{I}(\Delta,r,1/\sigma) - \mathcal{I}(\Delta,r,2/\sigma))]. \tag{14}$$

The bump radius may then be computed by finding the roots Δ of the equation $\kappa = \Psi(\Delta)$ with

$$\Psi(\Delta) = \frac{4\Delta}{3}\Big(I_1(\Delta)K_0(\Delta) - \frac{1}{2}I_1(2\Delta)K_0(2\Delta) - A(\sigma I_1(\Delta/\sigma)K_0(\Delta/\sigma) - \frac{\sigma}{2}I_1(2\Delta/\sigma)K_0(2\Delta\sigma))\Big). \tag{15}$$

Note that the threshold condition is a necessary but not sufficient condition for proving existence of a 2D bump. One also has to check that there are no other threshold crossing points. In the case of a Mexican or wizard hat weight distribution, there is typically a maximum of two spot solutions as illustrated in Fig. 2 for w given by Eq. (11). Using (9), we find that the narrower spot is always unstable as found in 1D. However, the stable upper branch can develop instabilities as the threshold is decreased leading to the formation of solutions that break the rotational symmetry [32, 39], see below.

Azimuthal Instabilities

It can be misleading to extrapolate results about bumps in 1D to spots in 2D. For example, it was known to Amari [1] in his seminal work on 1D models with Mexican hat weight distribution that bump solutions come in pairs, and that it is only the wider of the two that is stable. Extrapolating this to 2D, and focusing on radially symmetric spots, one would conclude a similar state of affairs for radial perturbations to the stationary spot, as done by John [48]. However, in the 2D setting one must also pay careful attention to azimuthal instabilities. This has been appreciated by a number of authors in recent years [20, 32, 39], though anticipated much earlier by Amari [3]. Indeed azimuthal instabilities can destabilise spots on the wide branch (that are stable to radial perturbations) and lead to the generation of intricate labyrinthine structures [16, 39].

In order to determine linear stability of a bump solution $U(r)$, substitute $u(\mathbf{r}, t) = U(r) + p(\mathbf{r})e^{\lambda t}$ into Eq. (1) and expand to first order in p using equation (4). This gives the eigenvalue equation

$$\begin{aligned}(\lambda+1)p(\mathbf{r}) &= \int w(|\mathbf{r}-\mathbf{r}'|)\delta(U(r')-\kappa))p(\mathbf{r}')\mathrm{d}\mathbf{r}' \\ &= \frac{1}{|U'(\Delta)|}\int_0^\infty\int_0^{2\pi} w(|\mathbf{r}-\mathbf{r}'|)\delta(r'-a)p(\mathbf{r}')\mathrm{d}\theta' r'\mathrm{d}r' \\ &= \frac{\Delta}{|U'(\Delta)|}\int_0^{2\pi} w(|\mathbf{r}-\mathbf{a}'|)p(a,\phi')\mathrm{d}\phi',\end{aligned} \tag{16}$$

where $\mathbf{a}' = (a, \phi')$. We can now formulate the stability problem in terms of finding the spectrum of a compact linear operator acting on continuous, bounded functions $\psi(r, \phi)$ defined on the disc of radius $r \le \Delta$. One class of solution to Eq. (16) consists of functions $p(\mathbf{r})$ that vanish on the boundary, $\psi(a,\phi) = 0$ for all ϕ, such that $\lambda = -1$. This belongs to the essential spectrum, which does not contribute to any instabilities. The discrete spectrum is determined by setting $\mathbf{r} = \mathbf{a} \equiv (\Delta, \phi)$ in Eq. (16):

$$(\lambda+1)p(\Delta,\phi) = \frac{\Delta}{|U'(\Delta)|}\int_0^{2\pi} w\left(2\Delta\sin\left(\frac{\phi-\phi'}{2}\right)\right)p(\Delta,\phi')\mathrm{d}\phi', \tag{17}$$

where we have simplified the argument of $w(r)$ using

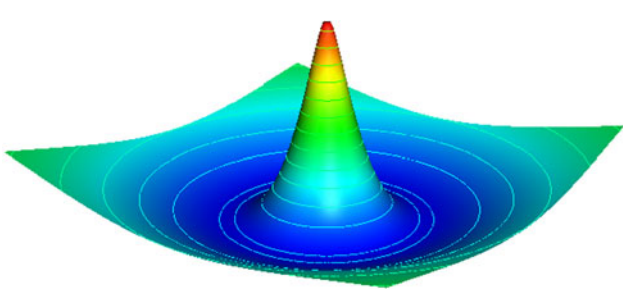

Fig. 1 A *plot* of the weight distribution describing short-range excitation and long-range inhibition. The form of $w(\mathbf{r})$ given by (11) with $A = 3/4$ and $\sigma = 4$ generates a two-dimensional wizard hat function

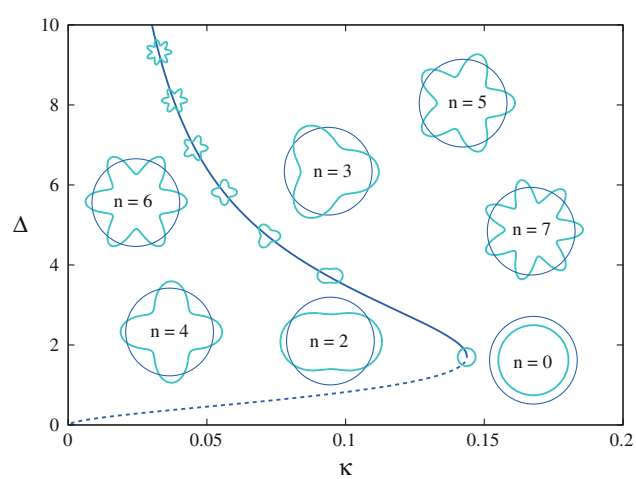

Fig. 2 The bump width Δ as a function of threshold κ, for the wizard hat weight distribution (11) with $A = 1/4$ and $\sigma = 2$, is shown by the continuous *dark blue line*. According to the linear radial instability analysis, the *solid* (*dashed*) *line* indicates a stable (unstable) branch of solutions. The azimuthal instability analysis predicts that solutions on the upper branch can also develop instabilities as the threshold is decreased leading to the formation of solutions exhibiting D_n symmetry. The points of azimuthal instability are marked by glyphs in the shape of the corresponding mode (Color figure online)

$$|\mathbf{a}-\mathbf{a}'| = \sqrt{2\Delta^2 - 2\Delta^2\cos(\phi-\phi')} = 2\Delta\sin\left(\frac{\phi-\phi'}{2}\right). \tag{18}$$

Equation (17) can be solved in terms of Fourier eigenmodes, that is, $p(\Delta,\phi) = P_n(\phi) = c_n e^{in\phi} + \bar{c}_n e^{-in\phi}$ with corresponding eigenvalue λ_n satisfying

$$\lambda_n = -1 + \frac{\Delta}{|U'(\Delta)|}\int_0^{2\pi} w(2\Delta\sin(\phi/2))e^{-in\phi}d\phi. \tag{19}$$

Note that λ_n is real since (after rescaling ϕ)

$$\mathrm{Im}\{\lambda_n\} = -\frac{2\Delta}{|U'(\Delta)|}\int_0^{\pi} w(2\Delta\sin(\phi))\sin(2n\phi)d\phi = 0, \tag{20}$$

i.e., the integrand is odd-symmetric about $\pi/2$. Hence,

$$\begin{aligned}\lambda_n &= \mathrm{Re}\{\lambda_n\}\\ &= -1 + \frac{\Delta}{|U'(\Delta)|}\int_0^{2\pi} w(2\Delta\sin(\phi/2))\cos(n\phi)d\phi,\end{aligned} \tag{21}$$

with the integrand even-symmetric about $\pi/2$. The Fourier eigenmodes $P_n(\phi)$ can be related to perturbations of the bump boundary. That is, if $u(\mathbf{r},t) = U(r) + \varepsilon\, p(\mathbf{r},t) = 0$ at $\mathbf{r} \equiv (r,\phi) = (\Delta + \varepsilon a(\phi,t),\phi)$, where $\varepsilon\, a(\phi,t)$ with $\varepsilon \ll 1$ denotes a small perturbation of the circular bump boundary at polar coordinate (Δ,ϕ) at time t, then

$$\begin{aligned}\kappa &= u(\Delta+\varepsilon a(\phi,t),\phi,t) = U(\Delta+\varepsilon a(\phi,t))\\ &\quad + \varepsilon p(\Delta+\varepsilon a(\phi,t),\phi,t),\\ &\approx U(\Delta) + \varepsilon U'(\Delta)a(\phi,t) + \varepsilon p(\Delta,\phi,t).\end{aligned} \tag{22}$$

Since $U(\Delta) = \kappa$, it follows that

$$a(\phi,t) \approx \frac{p(\Delta,\phi,t)}{|U'(\Delta)|}. \tag{23}$$

Thus, one can decompose time-dependent perturbations of the circular boundary in terms of the Fourier modes $[c_n e^{in\phi} + c_n e^{-in\phi}]e^{\lambda\, t}$. Some examples of perturbations of the bump boundary are shown as insets in Fig. 2. It can be seen that the nth-order boundary perturbation has D_n symmetry, meaning the resulting solution has the n reflectional and rotational symmetries of the dihedral group D_n. The perturbations also have a simple geometric interpretation. For example, $n = 0$ corresponds to a uniform expansion or contraction of the spot, whereas $n = 1$ corresponds to a uniform shift of the spot.

Since the $n = 1$ mode represents pure shifts of the spot solution, we expect $\lambda_1 = 0$ from translation symmetry. In order to verify this, we evaluate the integral appearing in equation (21) using Bessel functions, along similar lines to the evaluation of $U(r)$, Eq. (10). That is,

$$\begin{aligned}&\int_0^{2\pi} w(|\mathbf{a}-\mathbf{a}'|)\cos(n\phi')d\phi'\\ &= \int_0^{2\pi}\left(\int_0^{\infty}\widehat{w}(\rho)J_0(\rho|\mathbf{a}-\mathbf{a}'|)\rho d\rho\right)\cos\phi' d\phi'\\ &= 2\pi\int_0^{\infty}\widehat{w}(\rho)J_n(\rho\Delta)J_n(\rho\Delta)\rho d\rho.\end{aligned} \tag{24}$$

Moreover, differentiating Eq. (10) with respect to r gives

$$U'(\Delta) = -2\pi\Delta\int_0^{\infty}\widehat{w}(\rho)J_1(\Delta\rho)J_1(\Delta\rho)\rho d\rho. \tag{25}$$

Hence, the eigenvalue (21) can be rewritten as

$$\lambda_n = -1 + \frac{\int_0^{\infty}\widehat{w}(\rho)J_n(\rho r)J_n(\rho\Delta)\rho d\rho}{\int_0^{\infty}\widehat{w}(\rho)J_1(\rho r)J_1(\rho\Delta)\rho d\rho}. \tag{26}$$

It immediately follows that $\lambda_1 = 0$. Hence, the 2D spot is linearly stable if $\lambda_n < 0$ for all $n \neq 1$. For the weight distribution (11), the points of azimuthal stability as determined by the conditions $\lambda_n = 0$ can be calculated as [16]:

$$1 = \frac{\sum_{i=1}^{4} A_i K_n(\alpha_i\Delta)I_n(\alpha_i\Delta)}{\sum_{i=1}^{4} A_i K_1(\alpha_i\Delta)I_1(\alpha_i\Delta)}, \tag{27}$$

where $(A_1, A_2, A_3, A_4, \alpha_1, \alpha_2, \alpha_3, \alpha_4) = (1, -1, -A, A, 1, 2, 1/\sigma, 2/\sigma)$. In Fig. 2 we plot the set of points for $n = 0, 2, \ldots, 9$ as determined by equation (27) to illustrate how the upper branch of rotationally symmetric spots can become unstable as the threshold is decreased, leading to the formation of solutions that breaks continuous rotational symmetry. The discrete rotational symmetry D_n of a bifurcating solution reflects the order n of the dominant eigenvalue λ_n at bifurcation. Interestingly, if linear adaptation is included in the neural field model, then these nonrotationally symmetric solutions can undergo a secondary instability leading to the formation of a rotating wave [32, 39]. Sufficiently strong adaptation can also destabilise a bump leading to a travelling spot [15, 16]. An example of the shape of an expanding labyrinthine structure that can emerge when a spot destabilises to an $n = 3$ mode is shown in Fig. 3.

Stimulus-Induced Breathers

So far we have focused on activity bumps that persist in the absence of external stimuli due to the combined action of local recurrent excitation and lateral inhibition. We now describe some interesting instabilities that arise in the case

of nonpersistent bumps [20, 21]. For the sake of illustration, consider a 2D excitatory neural field with linear adaptation and an external input I:

$$\frac{\partial u(\mathbf{r},t)}{\partial t} = -u(\mathbf{r},t) + \int_{\mathbb{R}^2} w(|\mathbf{r}-\mathbf{r}'|)H(u(\mathbf{r}',t)-\kappa)\mathrm{d}\mathbf{r}' - \beta v(\mathbf{r},t) + I(\mathbf{r})$$
$$\frac{1}{\epsilon}\frac{\partial v(\mathbf{r},t)}{\partial t} = -v(\mathbf{r},t) + u(\mathbf{r},t), \tag{28}$$

where $v(\mathbf{r}, t)$ represents a local negative feedback mechanism, such as spike-rate adaptation, with ε, β determining the relative rate and strength of feedback [41]. Suppose that the inhomogeneous input is a radially symmetric Gaussian centred about the origin, $I(\mathbf{r}) = I_0 \mathrm{e}^{-r^2/\sigma_s^2}$. In the absence of an input, the resulting excitatory network supports travelling waves rather than stationary bumps. On the other hand, for sufficiently strong input amplitude I_0, the network supports a radially symmetric bump centred about the input. Such a bump is not persistent, since if the input is removed then the bump disappears as well. The basic problem we want to address is what happens to the stability of the bump as the input amplitude is slowly decreased.

The analysis of the existence and stability of radially symmetric 2D bumps proceeds as above with minor changes. First, the threshold condition for the existence of a bump becomes

$$\kappa = U(\Delta) = 2\pi\Delta \int_0^\infty \widehat{w}(\rho) J_0(\rho\Delta) J_1(\rho\Delta)\mathrm{d}\rho + I(\Delta). \tag{29}$$

Second, the linear stability of the bump is determined by the pair of eigenvalues $\lambda = \lambda_n^{\pm}$ associated with the Fourier modes $[c_n \mathrm{e}^{in\phi} + c_n \mathrm{e}^{-in\phi}]\mathrm{e}^{\lambda\, t}$, where [20]

$$\lambda_n^{\pm} = \frac{1}{2}\left[-\Lambda_n \pm \sqrt{\Lambda_n^2 - 4\epsilon(1+\beta)(1-\Gamma_n)}\right], \tag{30}$$

$$\Lambda_n = 1 + \epsilon - \Gamma_n(1+\beta), \quad \Gamma_n = \frac{\mu_n(\Delta)}{|U'(\Delta)|(1+\beta)}, \tag{31}$$

and

$$\mu_n(\Delta) = \Delta \int_0^{2\pi} w(2a\sin(\phi/2))\cos(n\phi)\mathrm{d}\phi. \tag{32}$$

It follows that stability of a radially symmetric bump require $\Lambda_n > 0$ and $\Gamma_n < 1$ for all $n \geq 0$. Given the form of Λ_n, this reduces to the following stability conditions:

$$\begin{array}{ll} \epsilon > \beta : \Gamma_n < 1 & \text{for all } n \geq 0 \\ \epsilon < \beta : \Gamma_n < \frac{1+\epsilon}{1+\beta} & \text{for all } n \geq 0. \end{array} \tag{33}$$

If the first condition is violated as some parameter is varied, then there is a saddle–node bifurcation, whereas a breakdown of the second condition signals a Hopf bifurcation. In the latter case, the bump instability leads to the formation of a breather. In the particular case of an excitatory network (such as obtained by setting $A = 0$ in Eq. (11)), with $w(r) \geq 0$ for all $r \geq 0$, we have

$$\mu_n \leq \Delta \int_0^{2\pi} w(2\Delta\sin(\phi/2))|\cos(n\phi)|\mathrm{d}\phi \leq \Delta \int_0^{2\pi} w(2\Delta\sin(\phi/2))\mathrm{d}\phi, \tag{34}$$

so that $\mu_n \leq \mu_0$ for all n. Since $\mu_1 = 0$, it follows that $\mu_0 \geq 0$ and, hence, a purely excitatory neural field cannot support stable radially symmetric bumps. In this case, we expect any instability to involve the growth of radially symmetric perturbations, and hence, the resulting breather will be radially symmetric. On the other hand, if there is a Mexican hat weight distribution, then nonradially symmetric breather and rotating waves can occur [21, 39]. One way to induce a Hopf instability of a bump is to reduce the amplitude I_0 of the Gaussian input; this modifies both the pulse-width Δ and the slope of the bump at threshold, $|U'(\Delta)|$. Interestingly, as the input amplitude is further reduced, the breather can undergo a

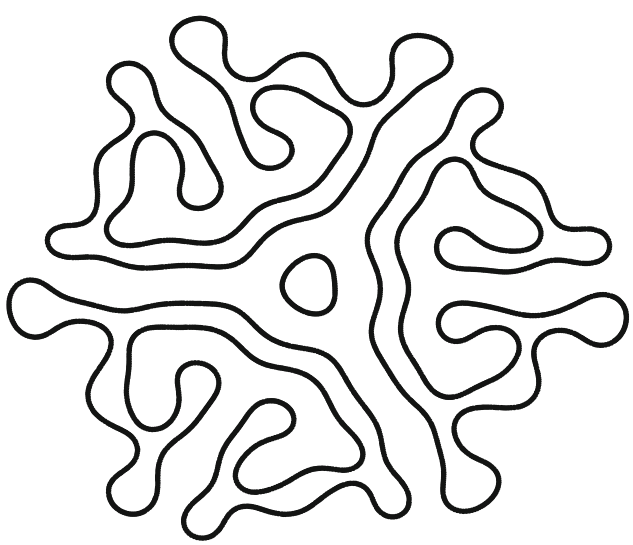

Fig. 3 Beyond the point of an azimuthal instability, direct numerical simulations of the neural field model show the development of intricate labyrinthine structures from an initial spot solution. Here we show the shape of such a structure at a fixed moment in time. As the pattern evolves, it fills more of the spatial domain. The *black lines* denote the borders between high and low firing regions. This example illustrates the type of pattern that one can expect to see beyond an $n = 3$ azimuthal instability. For further examples and discussion, see [16]

secondary instability such that it now acts as an oscillating core that emits circular target waves. An example of such a periodic wave emitter is shown in Fig. 4. Thus, a spatially localised stationary input provides a mechanism for the formation of a network pacemaker oscillator. For a recent discussion of breathers in the absence of localised input, see [15].

Self-Organising Neural Field Theory

One of the striking features of the visual system is that the visual world is mapped on to the cortical surface in a topographic manner. This means that neighbouring points in a visual image evoke activity in neighbouring regions of visual cortex. Superimposed upon this topographic map are additional maps reflecting the fact that neurons respond preferentially to stimuli with particular features such as ocular dominance and orientation [27]. In recent years, much information has accumulated regarding the two-dimensional distribution of both orientation preference and ocular dominance columns using optical imaging techniques [6, 7]. These experimental studies indicate that there is an underlying periodicity in the microstructure of V1 with a period of approximately 1 mm (in cats and primates). The fundamental domain of this tiling of the cortical plane is the hypercolumn, which contains two sets of orientation preferences $\theta \in [0,\pi)$ per eye, organised around a pair of orientation singularities or pinwheels [37]. It is generally accepted that the preference of cortical neurons for particular stimulus features such as orientation and ocular dominance arises primarily from the spatial arrangement of convergent feedforward afferents from the LGN (or from other layers of cortex). Although molecular cues and axon guidance are involved in the initial stages of cortical map formation, the resulting maps are rather crude and some form of spontaneous or stimulus-driven activity appears to be necessary for the subsequent refinement of these maps through the pruning of initially exuberant axonal arborisations.

A large number of models have been proposed that describe activity–dependent development as a self-organising Hebbian process (see the review of Swindale [44]). In the case of correlation–based developmental models [35], the statistical structure of input correlations provides a mechanism for spontaneously breaking some underlying symmetry of the neuronal receptive fields leading to the emergence of feature selectivity. When such correlations are combined with intracortical interactions, there is a simultaneous breaking of translation symmetry across cortex leading to the formation of a spatially periodic cortical feature map. Correlation-based models are essentially linear, so that considerable insight into the developmental process can be obtained by solving an associated eigenvalue problem [36]. One of the possible limitations of this class of model is that a regular topographic map is assumed already to exist before feature-based columns begin to develop. In order to model the joint development of topography and cortical feature maps, it appears necessary to introduce some form of nonlinear competition for activation [30, 52], neurotrophic factors [17], or a combination of the two [51].

An alternative mathematical formulation of topographic map formation has been developed by Amari using the theory of self–organising neural fields [2, 4, 45]. At the simplest level, this model can be formulated in terms of a two-layer network corresponding respectively to the lateral geniculate nucleus (LGN) of the thalamus and the primary visual cortex (see Fig. 5). The cortical or output layer behaves pretty much as in the single-layer model given by equation (1). However, the inputs I are now determined by activity in the LGN or input layer together with the strength of the feedforward connections from the LGN to cortex. These connections are modifiable by experience via Hebbian learning. Initially, an activity pattern in the form of a bump occurs at some random location within the LGN and elicits a corresponding activity bump in cortex whose location depends on the given pattern of feedforward connections. Over timescales much slower than the relaxation time τ for cortical dynamics, inputs arising from many different locations within LGN (and hence the visual image) occur. The resulting set of cortical responses to this set of inputs then

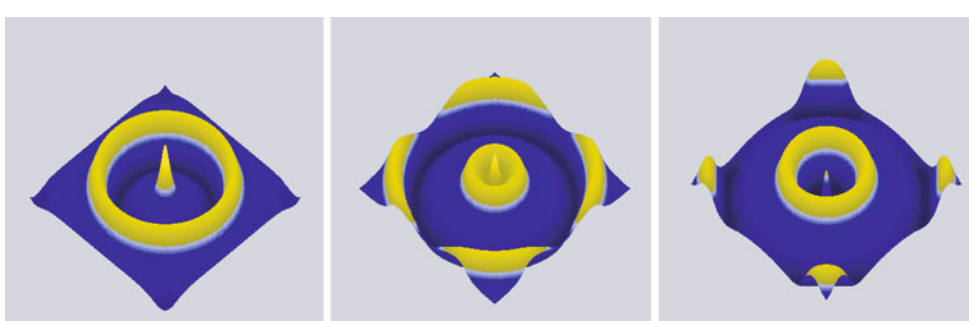

Fig. 4 Sequence of snapshots of a 2D breather acting as a periodic pulse emitter in the case of a 2D excitatory neural field with linear adaptation and exponential weight function $w(r) = e^{-r}/(2\ \pi)$. Parameters are $\beta = 4$, $\kappa = 0.2$, $\epsilon = 0.1$ and $I_0 = 0.2$. *Lighter colours* indicate higher activity [20]

determines how the feedforward weights are modified. In the one-dimensional case, Amari [45] derived conditions for the existence and stability of a continuous topographic map between the two layers. Moreover, he showed that under certain circumstances, the continuous topographic map can undergo a pattern-forming instability that spontaneously breaks continuous translation symmetry, and the map becomes partitioned into discretised blocks; it has been suggested that these blocks could be a precursor for the columnar microstructure of cortex [45]. Given that cortical columns tend to be associated with stimulus features such as ocular dominance and orientation, this raises the interesting question whether or not such features could also emerge through the spontaneous symmetry breaking of self-organising neural fields. In the same paper on bubble dynamics [48], John extended Amari's theory to 2D networks, again focusing on existence and stability with respect to radially symmetric perturbations. Stability with respect to a more general class of perturbations was subsequently analysed by Bressloff [8], who showed that stimulus preference maps could indeed emerge through the spontaneous symmetry breaking of self-organising neural fields. This analytical result was consistent with a number of numerical studies [19, 56]. In this section, we outline the basic steps in the analysis of 2D self-organising neural fields.

Existence and Stability of Bumps

Let $\mathbf{s} \in \Omega_2$ denote a point in the LGN layer and $\mathbf{r} \in \Omega_1$ a point in the cortical layer, as shown in Fig. 5. Each point $\mathbf{s}$ labels a distinct input pattern which we denote by $I(\mathbf{r}|\mathbf{s}), \mathbf{r} \in \Omega_1$. Let $u(\mathbf{r}|\mathbf{s})$ denote the corresponding cortical activity induced by the input $I(\mathbf{r}|\mathbf{s})$, which is assumed to converge to a stable equilibrium given by the solution of the integral equation

$$u(\mathbf{r}|\mathbf{s}) = \int_{\Omega_1} w(|\mathbf{r}-\mathbf{r}'|)H(u(\mathbf{r}'|\mathbf{s}) - \kappa)\mathrm{d}\mathbf{r}' + I(\mathbf{r}|\mathbf{s}). \tag{35}$$

Now suppose that once the network has reached equilibrium, a new input pattern is presented to the network from a different point $\mathbf{s}'$, and that this process is iterated multiple times so that the network samples over the space of inputs. How the network responds to the given set of input patterns then determines how these input patterns are themselves modified by experience. Adaptation is introduced into the model by assuming that the input patterns evolve according to the dynamical equation

$$\eta \frac{\partial I}{\partial t} = -I(\mathbf{r}|\mathbf{s}, t) + \int_{\Omega_2} g(|\mathbf{s}-\mathbf{s}'|)H(u(\mathbf{r}|\mathbf{s}', t) - \kappa)\mathrm{d}\mathbf{s}'. \tag{36}$$

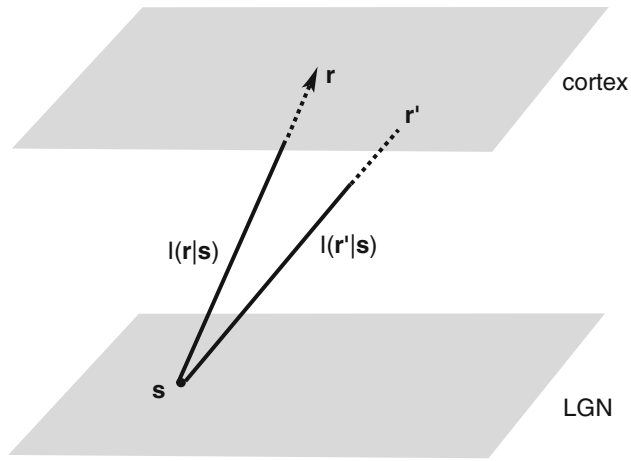

Fig. 5 Basic network architecture illustrating an input pattern I from position $\mathbf{s}$ in the LGN layer that innervates the cortical layer at different positions $\mathbf{r}$, $\mathbf{r}'$

Here $\eta \gg \tau$ where τ is the relaxation time for cortical dynamics. Hence, $u(\mathbf{r}|\mathbf{s}, t), \mathbf{r} \in \Omega_1$ denotes the equilibrium cortical state given by Eq. (35) in response to the input pattern $I(\mathbf{r}|\mathbf{s}, t)$ for fixed $\mathbf{s}, t$. The integral kernel g incorporates the effect of statistical correlations between activity patterns at different points in LGN. Thus, increasing the strength of an input from $\mathbf{s}$ also leads to an increase in the strength of an input at $\mathbf{s}'$ provided that $\mathbf{s}$ and $\mathbf{s}'$ are sufficiently close. Inputs from well-separated points in LGN are anticorrelated. These features can be included by taking g to be of the form

$$g(|\mathbf{r}|) = c\mathrm{e}^{-\mathbf{r}^2/4\sigma^2} - \hat{c} \tag{37}$$

for constants c, $\hat{c}$.

Equations (35) and (36) are the basic neural field equations for topographic map formation [2, 45]. Rescaling the LGN and cortical coordinates appropriately, that is, ignoring the effects of cortical magnification, one can then look for homogeneous steady–state solutions of the form $u(\mathbf{r}|\mathbf{s}) = U(|\mathbf{r} - \mathbf{s}|)$ and $I(\mathbf{r}|\mathbf{s}) = \bar{I}(|\mathbf{r}-\mathbf{s}|)$, where U is a radially symmetric stationary pulse solution of width a such that

$$\begin{aligned} U(|\mathbf{r}-\mathbf{s}|) &= \int_{\Omega_1} w(|\mathbf{r}-\mathbf{r}'|)H(U(|\mathbf{r}'-\mathbf{s}|) - \kappa)\mathrm{d}\mathbf{r}' \\ &\quad + \int_{\Omega_2} g(|\mathbf{s}-\mathbf{s}'|)H(U(|\mathbf{r}-\mathbf{s}'|) - \kappa)\mathrm{d}\mathbf{s}' \\ &= \int_0^{2\pi}\int_0^a [w(|\mathbf{r}-\mathbf{r}'|) + g(|\mathbf{r}-\mathbf{r}'|)]r'\mathrm{d}r'\mathrm{d}\theta, \end{aligned} \tag{38}$$

and

$$\bar{I}(|\mathbf{r}-\mathbf{s}|) = \int_{\Omega_2} g(|\mathbf{s}-\mathbf{s}'|)H(U(|\mathbf{r}-\mathbf{s}'|)-\kappa)\mathrm{d}\mathbf{s}'. \tag{39}$$

Such a solution represents a continuous topographic map in which an input from $\mathbf{s} \in \Omega_2$ is mapped to the centre of cortical output activity at the corresponding point $\mathbf{s} \in \Omega_1$. Stability of the bump (on the fast time–scale of cortical dynamics) can be analysed along identical lines to section 'Azimuthal Instabilities', after setting $\beta = 0$ and taking $w \to w + g$. The corresponding eigenvalues are $\lambda_n = -1 + \gamma^{-1} v_n$ with $|U'(a)| = \gamma$ and

$$v_n = a\int_0^{2\pi} [w(2a\sin(\theta/2)) + g(2a\sin(\theta/2))]\cos(n\theta)\mathrm{d}\theta. \tag{40}$$

Differentiating Eq. (4) with respect to r and setting $r = a$ shows that $v_1 = \gamma$ and, hence, $\lambda_1 = 0$. The existence of a zero eigenvalue reflects the underlying translation symmetry of the two-layer network, which implies that the bump is marginally stable with respect to uniform shifts in space. Thus, the bump will be stable provided that $v_n < \gamma$ for all $n \neq 1$. In the following, we assume that there exists a unique stable bump.

We now investigate the stability of the two–dimensional topographic map (on the slow timescale of the input or weights dynamics) by linearising Eqs. (35) and (36) about the homogeneous radially symmetric solution given by Eqs. (38) and (39). First, introducing the perturbations

$$\begin{aligned} u(\mathbf{r}|\mathbf{s},t) &= U(|\mathbf{r}-\mathbf{s}|) + p(\mathbf{r}|\mathbf{s},t), \\ I(\mathbf{r}|\mathbf{s},t) &= \bar{I}(|\mathbf{r}-\mathbf{s}|) + q(\mathbf{r}|\mathbf{s},t), \end{aligned} \tag{41}$$

and expanding to first order in p, q leads to the linear equations (on setting $\eta = 1$)

$$\frac{\partial q}{\partial t} = -q(\mathbf{r}|\mathbf{s},t) + \int_{R^2} g(|\mathbf{s}-\mathbf{s}'|)H'(U(|\mathbf{r}-\mathbf{s}'|)p(\mathbf{r}|\mathbf{s}',t)\mathrm{d}\mathbf{s}', \tag{42}$$

and

$$\begin{aligned} p(\mathbf{r}|\mathbf{s},t) = q(\mathbf{r}|\mathbf{s},t) &+ \int_{R^2} w(|\mathbf{r}-\mathbf{r}'|)H'(U(|\mathbf{r}'-\mathbf{s}|) \\ &\times p(\mathbf{r}'|\mathbf{s},t)\mathrm{d}\mathbf{r}'. \end{aligned} \tag{43}$$

Using the identity

$$H'(U(|\mathbf{r}-\mathbf{s}|) = \gamma^{-1}\delta(|\mathbf{r}-\mathbf{s}|-a), \tag{44}$$

we can reduce the above linear equations to the form

$$\frac{\partial q}{\partial t} = -q(\mathbf{r}|\mathbf{s},t) + \frac{a}{\gamma}\int_0^{2\pi} g(|\mathbf{s}-\mathbf{r}+a\mathbf{e}_\phi|)p(\mathbf{r}|\mathbf{r}-a\mathbf{e}_\phi,t)\mathrm{d}\phi, \tag{45}$$

and

$$\begin{aligned} p(\mathbf{r}|\mathbf{s},t) = q(\mathbf{r}|\mathbf{s},t) &+ \frac{a}{\gamma}\int_0^{2\pi} w(|\mathbf{r}-\mathbf{s}-a\mathbf{e}_\phi|)p \\ &\times (\mathbf{s}+a\mathbf{e}_\phi|\mathbf{s},t)\mathrm{d}\phi, \end{aligned} \tag{46}$$

with $\mathbf{e}_\theta = (\cos\theta, \sin\theta)$. Defining

$$p_\theta(\mathbf{s},t) = p(\mathbf{s}+a\mathbf{e}_\theta|\mathbf{s},t), \quad q_\theta(\mathbf{s},t) = q(\mathbf{s}+a\mathbf{e}_\theta|\mathbf{s},t), \tag{47}$$

and setting $\mathbf{r} = \mathbf{s} + a\mathbf{e}_\theta$ in Eq. (46), we find that

$$\begin{aligned} p_\theta(\mathbf{s},t) &= q_\theta(\mathbf{s},t) + \frac{a}{\gamma}\int_0^{2\pi} w(a|\mathbf{e}_\theta-\mathbf{e}_\phi|)p_\phi(\mathbf{s},t)\mathrm{d}\phi \\ &= q_\theta(\mathbf{s},t) + \frac{a}{\gamma}\int_0^{2\pi} w(2a\sin([\theta-\phi]/2)p_\phi(\mathbf{s},t)\mathrm{d}\phi. \end{aligned} \tag{48}$$

We have used the identity

$$|\mathbf{e}_\theta - \mathbf{e}_\phi|^2 = 2[1-\cos(\theta-\phi)] = 4\sin^2([\theta-\phi]/2). \tag{49}$$

Similarly, setting $\mathbf{r} = \mathbf{s} + a\mathbf{e}_\theta$ in Eq. (45) gives

$$\begin{aligned} \frac{\partial q_\theta}{\partial t} = -q_\theta(\mathbf{s},t) &+ \frac{a}{\gamma}\int_0^{2\pi} g(2a\sin([\theta-\phi]/2)p_\phi \\ &\times (\mathbf{s}+a(\mathbf{e}_\theta-\mathbf{e}_\phi),t)\mathrm{d}\phi. \end{aligned} \tag{50}$$

The neural field perturbations $p_\theta(\mathbf{r}, \tau)$ can be related to perturbations of the circular boundary of the activity bump. Let us write the perturbed threshold condition in the form $u(\mathbf{r}|\mathbf{s}, t) = \kappa$ at $\mathbf{r} = \mathbf{s} + (a + \rho(\theta, \xi, t))\mathbf{e}_\theta$. This yields

$$\begin{aligned} \kappa &= U(a+\rho(\theta,\xi,t)) + p(\mathbf{s}+(a+\rho(\theta,\mathbf{s},t))\mathbf{e}_\theta|\mathbf{s},t) \\ &= U(a) + U'(a)\rho(\theta,\mathbf{s},t) + p(\mathbf{s}+a\mathbf{e}_\theta|\mathbf{s},t) + \mathcal{O}(\rho^2), \end{aligned} \tag{51}$$

which implies that

$$\rho(\theta,\mathbf{s},t) = \gamma^{-1}p_\theta(\mathbf{s},t), \tag{52}$$

since $U(a) = \kappa$ and $U'(a) = -\gamma$. Here $\rho(\theta, \mathbf{s})$ represents the radial shift in the θ direction of the circular bump boundary centred at ξ and for fixed ξ corresponds directly

to the boundary perturbation considered in section 'Azimuthal Instabilities'.

Equations (48) and (50) have solutions of the form

$$p_\theta(\mathbf{s},t) = \mathrm{e}^{\lambda t}\mathrm{e}^{i\mathbf{k}\cdot\mathbf{s}}P_\theta(\mathbf{k}), \quad q_\theta(\mathbf{s},t) = \mathrm{e}^{\lambda t}\mathrm{e}^{i\mathbf{k}\cdot\mathbf{s}}Q_\theta(\mathbf{k}), \tag{53}$$

with

$$P_\theta(\mathbf{k}) = Q_\theta(\mathbf{k}) + \frac{a}{\gamma}\int_0^{2\pi} w(2a\sin([\theta-\phi]/2)P_\phi(\mathbf{k})\mathrm{d}\phi, \tag{54}$$

and

$$\lambda Q_\theta(\mathbf{k}) = -Q_\theta(\mathbf{k}) + \frac{a}{\gamma}\int_0^{2\pi} g(2a\sin([\theta-\phi]/2) \times \mathrm{e}^{ia\mathbf{k}\cdot(\mathbf{e}_\theta-\mathbf{e}_\phi)}P_\phi(\mathbf{k})\mathrm{d}\phi. \tag{55}$$

Equations (54) and (55) can be analysed further by introducing the Fourier series

$$P_\theta(\mathbf{k}) = \sum_{n\in\mathbf{Z}} P_n(\mathbf{k})\mathrm{e}^{in\theta}, \quad Q_\theta(\mathbf{k}) = \sum_{n\in\mathbf{Z}} Q_n(\mathbf{k})\mathrm{e}^{in\theta}. \tag{56}$$

This leads to the discrete set of equations

$$(\lambda+1)Q_n(\mathbf{k}) = \gamma^{-1}\sum_{n\in\mathbf{Z}} G_{nn'}(\mathbf{k})P_{n'}(\mathbf{k}), \tag{57}$$

$$P_n(\mathbf{k}) = \frac{Q_n(\mathbf{k})}{1-\gamma^{-1}\mu_n}, \tag{58}$$

with

$$G_{nn'}(\mathbf{k}) = a\int_0^{2\pi}\mathrm{e}^{-in\theta}\int_0^{2\pi}\mathrm{e}^{in'\phi}g(2a\sin([\theta-\phi]/2) \times \mathrm{e}^{ia\mathbf{k}\cdot(\mathbf{e}_\theta-\mathbf{e}_\phi)}\frac{\mathrm{d}\phi\mathrm{d}\theta}{2\pi}, \tag{59}$$

and

$$\mu_n = a\int_0^{2\pi} w(2a\sin(\theta/2))\cos(n\theta)\mathrm{d}\theta. \tag{60}$$

Calculation of Eigenmodes

Determining the stability of the two-dimensional topographic map has reduced to the problem of finding the eigenvalues of the infinite-dimensional matrix $G_{nn'}(\mathbf{k})$ for $n, n' \in \mathbf{Z}$. It is not possible to do this analytically for general input kernel g. However, an explicit solution can be obtained in the limiting case of wide Gaussian inputs such that $\sigma \gg a$ in Eq. (37). We can then carry out a perturbation expansion in a^2/σ^2 by writing

$$g(2a\sin(\theta/2)) = c\mathrm{e}^{-a^2\sin^2(\theta/2)/\sigma^2} - \hat{c} \approx c - \hat{c} - \frac{ca^2}{2\sigma^2}(1-\cos(\theta)) + \mathcal{O}(a^4/\sigma^4). \tag{61}$$

Keeping only lowest order terms, we find that

$$G_{nn'}(\mathbf{k}) \approx a(c-\hat{c})\int_0^{2\pi}\mathrm{e}^{-in\theta}\int_0^{2\pi}\mathrm{e}^{in'\phi}\mathrm{e}^{iak(\cos(\theta-\varphi)-\cos(\phi-\varphi))}\frac{\mathrm{d}\phi\mathrm{d}\theta}{2\pi}, \tag{62}$$

where $\mathbf{k} = (k, \varphi)$ in polar coordinates. The integrals over ϕ and θ may now be evaluated using the following Bessel function expansion:

$$\mathrm{e}^{ika\cos(\theta-\varphi)} = \sum_{m\in\mathbf{Z}}(-i)^m J_m(ka)\mathrm{e}^{im(\theta-\varphi)}, \tag{63}$$

with $J_{-m} = J_m$. This gives

$$\begin{aligned} G_{nn'}(\mathbf{k}) &\approx a(c-\hat{c})\int_0^{2\pi}\mathrm{e}^{-in\theta}\int_0^{2\pi}\mathrm{e}^{in'\phi}\sum_{m\in\mathbf{Z}}(-i)^m J_m(ka)\mathrm{e}^{im(\theta-\varphi)} \\ &\quad\times\sum_{m'\in\mathbf{Z}}(i)^{m'}J_{m'}(ka)\mathrm{e}^{-im'(\phi-\varphi)}\frac{\mathrm{d}\phi\mathrm{d}\theta}{2\pi} \\ &= 2\pi a(c-\hat{c})(-i)^n(i)^{n'}J_n(ka)J_{n'}(ka)\mathrm{e}^{i(n'-n)\varphi}. \end{aligned} \tag{64}$$

Similarly, substituting Eq. (61) into (40) and gives to lowest order

$$\mu_0 \approx \nu_0 - 2\pi a(c-\hat{c}), \quad \mu_1 \approx \nu_1 - \pi ac\frac{a^2}{2\sigma^2}, \quad \mu_n \approx \nu_n, \quad n > 1. \tag{65}$$

Combining Eqs. (57), (58), and (64) yields a vector equation of the form

$$\mathbf{b}^*(\mathbf{k})(\mathbf{b}(\mathbf{k})\cdot\widehat{\mathbf{P}}(\mathbf{k})) = (1+\lambda)\widehat{\mathbf{P}}(\mathbf{k}), \tag{66}$$

where * denotes complex conjugate, and

$$\begin{aligned} \widehat{P}_n(\mathbf{k}) &= \sqrt{\gamma-\mu_n}P_n(\mathbf{k}), \\ b_n(\mathbf{k}) &= \sqrt{\frac{2\pi a(c-\hat{c})}{\gamma-\mu_n}}(i)^n J_n(ka)\mathrm{e}^{in\varphi}. \end{aligned} \tag{67}$$

There are two classes of solution to Eq. (66). If $\mathbf{b}\cdot\widehat{\mathbf{P}} = 0$ then $\lambda = -1$ and the topographic map is stable with respect to excitation of the corresponding eigenmodes. On the other hand, if $\mathbf{b}\cdot\widehat{\mathbf{P}} \neq 0$ then $\widehat{\mathbf{P}} = \mathbf{b}^*$ (up to a constant multiplicative factor). Substituting into the Fourier series (56), the resulting eigenmode is of the form $P_\theta(\mathbf{k}) = P(k, \theta-\varphi)$ with $\mathbf{k} = (k, \varphi)$,

$$P(k,\theta) = \Gamma\left[\frac{J_0(ka)}{\gamma-\mu_0} + 2\sum_{n\geq 1}(-1)^n\frac{J_{2n}(ka)}{\gamma-\mu_{2n}}\cos(2n\theta) - 2\sum_{n\geq 1}(-1)^n\frac{J_{2n-1}(ka)}{\gamma-\mu_{2n-1}}\sin((2n-1)\theta)\right], \tag{68}$$

where Γ is an arbitrary amplitude. The corresponding eigenvalue is $\lambda = \lambda(k)$ with

$$\lambda(k) = -1 + |\mathbf{b}|^2 = -1 + \sum_{n\in\mathbf{Z}}\frac{2\pi a(c-\hat{c})}{\Gamma-\mu_n}J_n(ka)^2. \tag{69}$$

For the sake of illustration, suppose that $\mu_n < \gamma$ for all $n \in \mathbf{Z}$. This is plausible given Eq. (65) and the conditions on μ_n. Equation (69) implies that if $c<\hat{c}$ then the topographic map is stable since $\lambda(k) < 0$ for all k. On the other hand, if $c > \hat{c}$ such that $\lambda(k_c) = \max_{\lambda k}(k) > 0$ then the topographic map is unstable and the fastest growing eigenmodes have the critical wavenumber k_c. Recall that $\gamma = \nu_1$. It then follows from Eq. (65) that $\mu_1 \approx \gamma$ and the dominant contribution to the sum in Eq. (69) will arise from the $n = 1$ term, at least away from the zeros of $J_1(ka)$. Hence, k_c is approximately given by the point at which the first-order Bessel function attains its global maximum, that is, $|J_1(ak_c)| = \max_k |J_1(ak)|$. Numerically one finds that $k_c \approx 3/a$. Note that the eigenvalues $\lambda(k)$, $k \neq 0$, have an infinite degeneracy that reflects the additional rotation symmetry of the system. That is, all eigenmodes $P_\theta(\mathbf{k})$ with $|\mathbf{k}| = k$ have the same eigenvalue. It follows that the pattern-forming instability will be dominated by some linear combination of eigenmodes lying on the critical circle $|\mathbf{k}| = k_c$:

$$p_\theta(\mathbf{r}) = \sum_{i=1}^{N}\left(z_i e^{i\mathbf{k}_i\cdot\mathbf{r}} + z_i^* e^{i\mathbf{k}_i\cdot\mathbf{r}}\right)P(k_c,\theta-\varphi_i), \tag{70}$$

where $\mathbf{k}_i = (k_c, \varphi_i)$ and z_i is a complex amplitude. Suppose that each eigenmode can be approximated by the first three terms of Eq. (68) so that

$$P(k_c,\theta) \approx \Gamma\left[\frac{J_0(k_c a)}{\gamma-\mu_0} + \frac{2J_1(k_c a)}{\gamma-\mu_1}\sin(\theta) - \frac{2J_2(k_c a)}{\gamma-\mu_2}\cos(2\theta)\right]. \tag{71}$$

The first term generates an expansion of the bump, the second term generates a uniform shift of the bump, and the third term generates an elongation of the bump (see Fig. 2). In general, we expect the eigenmode (71) to be dominated by the first harmonic term $\sin(\theta)$, since $\mu_1 \approx \gamma$. However, if $\mu_2 \approx \gamma$ as well, then there could also be a significant contribution from the term $\cos(2\theta)$. Thus, the spontaneous symmetry breaking mechanism has the potential for generating elongated or oriented bumps. Moreover, since each eigenmode in the sum (70) then represents an elongation in the direction φ_i or $\pi/2 + \varphi_i$ (depending on the sign of its associated coefficient $z(\mathbf{r}) = z_i e^{i\mathbf{k}_i\cdot\mathbf{r}} + z_i^* e^{i\mathbf{k}_i\cdot\mathbf{r}}$), it follows that there is some complicated variation in the preferred bump orientation as $\mathbf{r}$ varies across the cortex.

Euclidean Shift-Twist Symmetry and Orientation Preference Maps

The two-dimensional isotropic and homogeneous neural field Eqs. (35) and (36) are equivariant with respect to the product Euclidean group $\mathbf{E}(2) \times \mathbf{E}(2)$ acting on the space $\mathbf{R}^2 \times \mathbf{R}^2$ according to

$$\begin{aligned} T_{\mathbf{d},\mathbf{d}'}\cdot(\mathbf{r},\mathbf{s}) &= (\mathbf{r}+\mathbf{d},\mathbf{s}+\mathbf{d}'),\\ R_{\xi,\xi'}\cdot(\mathbf{r},\mathbf{s}) &= (R_\xi\mathbf{r},R_{\xi'}\mathbf{s}),\\ R_{\kappa,\kappa'}\cdot(\mathbf{r},\mathbf{s}) &= (R_\kappa\mathbf{r},R_{\kappa'}\mathbf{s}), \end{aligned} \tag{72}$$

where $R_\xi\mathbf{r}$ denotes the planar rotation of $\mathbf{r}$ through an angle ξ, and $R_\kappa = R_\pm$ with $R_\pm(x, y) = (x, \pm y)$. The corresponding group action on the neural fields u, I is

$$\begin{aligned} T_{\mathbf{d},\mathbf{d}'}(u(\mathbf{r}|\mathbf{s}),I(\mathbf{r}|\mathbf{s})) &= (u(\mathbf{r}-\mathbf{d}|\mathbf{s}-\mathbf{d}'),I(\mathbf{r}-\mathbf{d}|\mathbf{s}-\mathbf{d}'))),\\ R_{\xi,\xi'}(u(\mathbf{r}|\mathbf{s}),I(\mathbf{r}|\mathbf{s})) &= (u(R_{-\xi}\mathbf{r}|R_{-\xi'}\mathbf{s}),I(R_{-\xi}\mathbf{r}|R_{-\xi'}\mathbf{s})),\\ R_{\kappa,\kappa'}(u(\mathbf{r}|\mathbf{s}),I(\mathbf{r}|\mathbf{s})) &= (u(R_\kappa\mathbf{r}|R_{\kappa'}\mathbf{s}),I(R_\kappa\mathbf{r}|R_{\kappa'}\mathbf{s})). \end{aligned} \tag{73}$$

Equivariance means that if (u, v) is a solution of the neural field equations then so is $\eta\cdot(u,v)$ for all $\eta \in \mathbf{E}(2)\times\mathbf{E}(2)$. In other words, the two-dimensional network has both translation and rotation/reflection symmetries. An isotropic and homogeneous equilibrium solution of the form $u(\mathbf{r}_2|\mathbf{r}) = U(|\mathbf{r}_2-\mathbf{r}|), I(\mathbf{r}_2|\mathbf{r}) = \bar{I}(|\mathbf{r}_2-\mathbf{r}|)$ then explicitly breaks the symmetry group from $\mathbf{E}(2)\times\mathbf{E}(2) \to \mathbf{E}(2)$ with $\mathbf{E}(2)$ having the group elements $T_\mathbf{d} = T_\mathbf{d}$, $\mathbf{d}$, $R_\xi = R_{\xi,\xi}$ and $R_\kappa = R_{\kappa,\kappa}$. As we have shown above, the homogeneous equilibrium solution can undergo a pattern-forming instability that spontaneously breaks the remaining Euclidean symmetry.

The Euclidean symmetry of the full Eqs. (35) and (36) also manifests itself in a reduced form after linearising about the homogeneous solution. That is, the linear equations (48) and (50) are equivariant with respect to the so-called shift-twist action of the Euclidean group $\mathbf{E}(2)$ on the space $\mathbf{R}^2 \times S^1$ [10, 11]:

$$\begin{aligned} T_\mathbf{d}\cdot(\mathbf{r},\theta) &= (\mathbf{r}+\mathbf{d},\theta),\\ R_\xi\cdot(\mathbf{r},\theta) &= (R_\xi\mathbf{r},\theta+\mathbf{s}),\\ R_\kappa\cdot(\mathbf{r},\theta) &= (R_\kappa\mathbf{r},-\theta), \end{aligned} \tag{74}$$

where $R_\kappa(x, y) = (x, -y)$. The corresponding action on the fields $p_\theta(\mathbf{r})$ and $q_\theta(\mathbf{r})$ is

$$\begin{aligned} T_\mathbf{d}\cdot(p_\theta(\mathbf{r}),q_\theta(\mathbf{r})) &= (p_\theta(\mathbf{r}-\mathbf{d}),q_\theta(\mathbf{r}-\mathbf{d})),\\ R_\xi\cdot(p_\theta(\mathbf{r}),q_\theta(\mathbf{r})) &= (p_{\theta-\xi}(R_{-\xi}\mathbf{r}),q_{\theta-\xi}(R_{-\xi}\mathbf{r})),\\ R_\kappa\cdot(p_\theta(\mathbf{r}),q_\theta(\mathbf{r})) &= (p_{-\theta}(R_\kappa\mathbf{r}),q_{-\theta}(R_\kappa\mathbf{r})). \end{aligned} \tag{75}$$

It can be seen that the rotation operation comprises a translation or *shift* of the angle θ to $\theta + \mathbf{s}$, together with a rotation or *twist* of the position vector $\mathbf{r}$ by the angle $\mathbf{s}$. This is illustrated in Fig. 6. One of the consequences of the underlying Euclidean symmetry is that the associated eigenfunctions form irreducible representations of the shift-twist group action [10, 11]. This explains why the eigenmodes $P_\theta(\mathbf{k})$ have the basic structure given by equation (68), with the angular variable θ coupled to the direction of the wavevector $\mathbf{k}$.

The emergence of elongated cortical activity bumps reflects a corresponding elongation in the receptive field properties of cortical cells. Hence, the spontaneous symmetry breaking of the topographic map between LGN and visual cortex provides a possible mechanism for the development of orientation preference columns in primary visual cortex. The variation in orientation with cortical position then determines the corresponding orientation preference map. Interestingly, a recent statistical analysis of orientation preference maps in primates indicates that there are correlations between the direction of the topographic axis joining pairs of columns with similar orientation preferences and their common orientation [34]. Thus, the orientation preference map exhibits a form of rotational shift-twist symmetry as predicted from our analysis of two-dimensional topographic maps. Numerical simulations of a feature-based dynamical spin model has led to the suggestion that such a symmetry could help to stabilise the emerging orientation preference map with its associated set of pinwheels [34]. As previously shown by Wolf and Geisel [55], in the absence of such a coupling, the pinwheels typically annihilate in pairs. Hence, in order to maintain pinwheels, either development has to be stopped or one has to introduce inhomogeneities that trap the pinwheels.

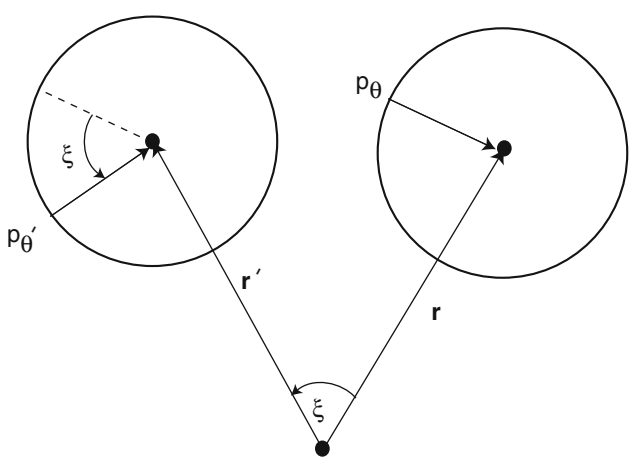

Fig. 6 Action of a rotation by $\xi : p_\theta(\mathbf{r}) \to p_{\theta'}(\mathbf{r}')$ where $(\mathbf{r}', \theta') = (R_\xi \mathbf{r}, \theta + \xi)$. Here $\mathbf{r}$ represents the position of the centre of a two-dimensional bump and p_θ represents the perturbation of steady-state activity at a point θ on the boundary of the bump

Discussion

In this review, we have described John G Taylor's work on neural bubble dynamics [48], as well as various extensions that have revealed a rich repertoire of 2D network dynamics, including breathers [15, 20, 39], multiple bumps [32], labyrinthine structures [16, 39], rotating waves [21], spiral waves [26, 29, 31, 43], and travelling spots [15, 16]. Traditionally, in vitro methods for studying the generation and propagation of electrical activity in networks of neurons have involved removing a thin vertical slice of brain tissue [13, 23, 40, 42], which makes it difficult to observe the various forms of 2D dynamics predicted by neural field theory. However, recent studies of tangential slices have demonstrated that various phenomena predicted by neural field theory are also observed in living tissue [26, 57]. Interestingly the type of neural field models discussed here (and their localised solutions) has been adopted as a formal framework for thinking about embodied cognitive dynamics by Gregor Schöner and colleagues, see for example [28]. Initially, this work focused on developing a theory of how eye movements are planned, though has since been expanded to a variety of topics including motor planning and visuospatial cognition. Moreover, the same style of conceptual modelling has proven fruitful in developing a theory of cognitive robotics [18]. There is clearly still much to be gained by the mathematical study of neural field models along the lines developed by John G Taylor and others.

Open Access This article is distributed under the terms of the Creative Commons Attribution License which permits any use, distribution, and reproduction in any medium, provided the original author(s) and the source are credited.

Appendix

The double integral in (3) can be calculated using Fourier transforms and Bessel function identities [20]. First, express $w(r)$ as a 2D Fourier transform using polar coordinates:

$$w(r) = \frac{1}{2\pi} \int_{\mathbb{R}^2} \mathrm{e}^{i\mathbf{r}\cdot\mathbf{k}} \widehat{w}(\mathbf{k}) \mathrm{d}\mathbf{k} = \frac{1}{2\pi} \int_0^\infty \left(\int_0^{2\pi} \mathrm{e}^{ir\rho\cos\theta} \widehat{w}(\rho) \mathrm{d}\theta \right) \rho \mathrm{d}\rho, \tag{76}$$

where $\widehat{w}$ denotes the Fourier transform of w and $\mathbf{k} = (\rho, \theta)$. Using the integral representation

$$\frac{1}{2\pi}\int_0^{2\pi} \mathrm{e}^{ir\rho\cos\theta}\mathrm{d}\theta = J_0(\rho r), \tag{77}$$

where J_0 is the Bessel function of the first kind, we express w in terms of its Hankel transform of order zero,

$$w(r) = \int_0^{\infty} \widehat{w}(\rho)J_0(\rho r)\rho\mathrm{d}\rho, \tag{78}$$

which, when substituted into Eq. (4), gives

$$U(r) = \int_0^{2\pi}\int_0^{\Delta}\left(\int_0^{\infty} \widehat{w}(\rho)J_0(\rho|\mathbf{r}-\mathbf{r}'|)\rho\mathrm{d}\rho\right) r'\mathrm{d}r'\mathrm{d}\phi'. \tag{79}$$

Reversing the order of integration and using the addition theorem

$$J_0\left(\rho\sqrt{r^2+r'^2-2rr'\cos\phi'}\right) = \sum_{m=0}^{\infty}\epsilon_m J_m(\rho r)J_m(\rho r')\cos m\phi', \tag{80}$$

where $\epsilon_0 = 1$ and $\epsilon_n = 2$ for $n \geq 1$, we thus obtain (10), using the identity $J_1(\rho\Delta)\Delta = \rho\int_0^{\Delta} J_0(\rho r')r'\mathrm{d}r'$.

References

1. Amari S. Dynamics of pattern formation in lateral-inhibition type neural fields. Biol Cybern. 1977;27:77–87.
2. Amari S. Topographic organization of nerve fields. Bull Math Biol. 1980;42:339–64.
3. Amari SI. Mathematical theory of nerve nets. Sangyotosho; 1978.
4. Amari SI. Field theory of self-organizing neural nets. IEEE Trans Syst Man Cybern. 1983;13:741–8.
5. Amari SI. Neural field theory, chap. Heaviside world: excitation and self-organization of neural fields. Springer; 2013.
6. Blasdel GG, Salama G. Voltage-sensitive dyes reveal a modular organization in monkey striate cortex. Nature. 1986;321:579–85.
7. Bonhoeffer T, Grinvald A. Iso-orientation domains in cat visual cortex are arranged in pinwheel-like patterns. Nature. 1991; 353:429–31.
8. Bressloff PC. Spontaneous symmetry breaking in self-organizing neural fields. Biol Cybern. 2005;93:256–74.
9. Bressloff PC. Spatiotemporal dynamics of continuum neural fields. J Phys A: Math Theor. 2012;45:033001.
10. Bressloff PC, Cowan JD, Golubitsky M, Thomas PJ. Scalar and pseudoscalar bifurcations: pattern formation on the visual cortex. Nonlinearity. 2001;14:739–75.
11. Bressloff PC, Cowan JD, Golubitsky M, Thomas PJ, Wiener M Geometric visual hallucinations, euclidean symmetry and the functional architecture of striate cortex. Philos Trans R Soc Lond B. 2001;356:299–330.
12. Camperi M, Wang XJ. A model of visuospatial short-term memory in prefrontal cortex: recurrent network and cellular bistability. J Comput Neurosci. 1998;5:383–405.
13. Chervin RD, Pierce PA, Connors BW. Periodicity and directionality in the propagation of epileptiform discharges across neocortex. J Neurophysiol. 1988;60:1695–713.
14. Coombes S. Waves, bumps, and patterns in neural field theories. Biol Cybern. 2005;93:91–108.
15. Coombes S, Schmidt H, Avitabile D. Neural field theory, chap. Spots: breathing, drifting and scattering in a neural field model. Springer; 2013.
16. Coombes S, Schmidt H, Bojak I. Interface dynamics in planar neural field models. J Math Neurosci. 2012;2(9).
17. Elliott T, Shadbolt NR. A neurotrophic model for the development of the retinogeniculocortical pathway induced by spontaneous retinal waves. J Neurosci. 1999;19:7951–70.
18. Erlhagen W, Bicho E. The dynamic neural field approach to cognitive robotics. J Neural Eng. 2006;3:R36–54.
19. Fellenz WA, Taylor JG. Establishing retinotopy by lateral-inhibition type homogeneous neural fields. Neurocomputing. 2002; 48:313–22.
20. Folias SE, Bressloff PC. Breathing pulses in an excitatory neural network. SIAM J Appl Dyn Syst. 2004;3(3):378–407.
21. Folias SE, Bressloff PC. Breathers in two-dimensional neural media. Phys Rev Lett. 2005;95:208107(1–4).
22. Fuster JM, Alexander G. Neuron activity related to short-term memory. Science. 1971;173:652.
23. Golomb D, Amitai Y. Propagating neuronal discharges in neocortical slices: computational and experimental study. J Neurophysiol. 1997;78:1199–211.
24. Gutkin B, Laing CR, Colby CL, Chow CC, Ermentrout GB. Turning on and off with excitation: the role of spike-timing asynchrony and synchrony in sustained neural activity. J Comput Neurosci. 2001;11:121–34.
25. Herrmann JM, Schrobsdorff H, Geisel T. Localized activations in a simple neural field model. Neurocomputing. 2005;65:679–84.
26. Huang X, Troy WC, Yang Q, Ma H, Laing CR, Schiff SJ, Wu J. Spiral waves in disinhibited mammalian neocortex. J Neurosci. 2004;24:9897–902.
27. Hubel DH, Wiesel TN. Functional architecture of macaque monkey visual cortex. Philos Trans R Soc Lond B Biol Sci. 1977;198:1–59.
28. Johnson JS, Spencer JP, Schöner G Moving to higher ground: the dynamic field theory and the dynamics of visual cognition. New Ideas Psychol. 2008;26(2):227–51.
29. Kilpatrick ZP, Bressloff PC. Spatially structured oscillations in a two-dimensional neuronal network with synaptic depression. J Comput Neurosci. 2010;28:193–209.
30. Kohonen T. Self-organized formation of topologically correct feature maps. Biol Cybern. 1982;43:59–69.
31. Laing CR. Spiral waves in nonlocal equations. SIAM J Appl Dyn Syst. 2005;4:588–606.
32. Laing CR, Troy WC. PDE methods for nonlocal models. SIAM J Appl Dyn Syst. 2003;2:487–516.
33. Laing CR, Troy WC, Gutkin B, Ermentrout GB. Multiple bumps in a neuronal model of working memory. SIAM J Appl Math. 2002;63:62–97.
34. Lee HY, Yahyanejad M, Kardar M. Symmetry considerations and development of pinwheels in visual maps. Proc Nat Acad Sci USA. 2003;100:16036–40.
35. Miller KD, Keller JB, Stryker MP. Ocular dominance column development: analysis and simulation. Science. 1989;245:605–14.
36. Miller KD, Mackay DJC. The role of constraints in Hebbian learning. Neural Comput. 1994;6:100–26.
37. Obermayer K, Blasdel GG. Geometry of orientation and ocular dominance columns in monkey striate cortex. J Neurosci. 1993; 13:4114–29.

38. O'Keefe J, Recce ML. Phase relationship between hippocampal place units and the EEG theta rhythm. Hippocampus. 1993;3:317–30.
39. Owen MR, Laing CR, Coombes S. Bumps and rings in a two-dimensional neural field: splitting and rotational instabilities. New J Phys. 2007;9:378.
40. Pinto D, Patrick SL, Huang WC, Connors BW. Initiation, propagation, and termination of epileptiform activity in rodent neocortex in vitro involve distinct mechanisms. J Neurosci. 2005;25:8131–40.
41. Pinto DJ, Ermentrout GB. Spatially structured activity in synaptically coupled neuronal networks: I. Traveling fronts and pulses. SIAM J Appl Math. 2001;62:206–25.
42. Richardson KA, Schiff SJ, Gluckman BJ. Control of traveling waves in the mammalian cortex. Phys Rev Lett. 2005;94:028103.
43. Shusterman V, Troy WC. From baseline to epileptiform activity: a path to synchronized rhythmicity in large-scale neural networks. Phys Rev E. 2008;77:061911.
44. Swindale NV. The development of topography in the visual–cortex: a review of models. Network 1996;7:161–274.
45. Takeuchi A, Amari S. Formation of topographic maps and columnar microstructures in nerve fields. Biol Cybern. 1979;35:63–72.
46. Taube JS, Bassett JP. Persistent neural activity in head direction cells. Cereb Cortex. 2003;13:1162–72.
47. Taylor JG. Black holes: the end of the universe? New York: Random House; 1973.
48. Taylor JG. Neural 'bubble' dynamics in two dimensions: Foundations. Biol Cybern. 1999;80:393–409.
49. Taylor JG, Bressloff PC, Restuccia A. Finite superstrings. Singapore: World Scientific; 1992.
50. Werner H, Richter T. Circular stationary solutions in two-dimensional neural fields. Biol Cybern. 2001;85:211–7.
51. Whitelaw VA, Cowan JD. Specificity and plasticity of retinotectal connections: a computational model. J Neurosci. 1981;1:1369–87.
52. Willshaw DJ, von der Malsburg C. How patterned neural connections can be set up by self-organization. Proc R Soc Lond B Biol Sci. 1976;194:431–45.
53. Wilson HR, Cowan JD. Excitatory and inhibitory interactions in localized populations of model neurons. Biophys J. 1972;12:1–24.
54. Wilson HR, Cowan JD. A mathematical theory of the functional dynamics of cortical and thalamic nervous tissue. Kybernetik. 1973;13:55–80.
55. Wolf F, Geisel T. Spontaneous pinwheel annihilation during visual development. Nature. 1998;395:73–8.
56. Woodbury GA, van der Zwan R, Gibson WG. Correlation model for joint development of refined retinotopic map and ocular dominance columns. Vision Res. 2002;42:2295–310.
57. Wu J. Propagating waves of activity in the neocortex: what they are, what they do. Neuroscientist. 2008;14:487–502.